Numerical analysis of a neutrally buoyant spheroid rotating in shear at small Reynolds numbers

T. Rosén,[1,2] J. Einarsson,[3] A. Nordmark,[1] C. K. Aidun,[4] F. Lundell,[1,2] and B. Mehlig[3]
[1)] *KTH Mechanics, Royal Institute of Technology, SE-100 44 Stockholm, Sweden*
[2)] *Wallenberg Wood Science Center, Royal Institute of Technology, SE-100 44 Stockholm, Sweden*
[3)] *Department of Physics, Gothenburg University, 41296 Gothenburg, Sweden*
[4)] *George W. Woodruff School of Mechanical Engineering, and Parker H. Petit Institute for Bioengineering and Bioscience 801 Ferst Drive, Georgia Institute of Technology, Atlanta, GA 30332-0405*

We numerically analyse the rotation of a neutrally buoyant spheroid in a shear flow at small shear Reynolds number. Using direct numerical stability analysis of the coupled nonlinear particle-flow problem we compute the linear stability of the log-rolling orbit at small shear Reynolds number, Re_a. As $\mathrm{Re}_a \to 0$ and as the box size of the system tends to infinity we find good agreement between the numerical results and earlier analytical predictions valid to linear order in Re_a for the case of an unbounded shear. The numerical stability analysis indicates that corrections to the analytical result are of order $\mathrm{Re}_a^{3/2}$. We also compare the analytical results to results of lattice-Boltzmann simulations to analyse the stability of the tumbling orbit at shear Reynolds numbers of order unity. Theory for an unbounded system at infinitesimal shear Reynolds number predicts a bifurcation of the tumbling orbit at aspect ratio $\lambda_c \approx 0.137$ below which tumbling is stable (as well as log rolling). The simulation results show a bifurcation line in the λ-Re_a plane that reaches $\lambda \approx 0.1275$ at the smallest shear Reynolds number at which we could simulate, $\mathrm{Re}_a = 1$, in qualitative agreement with the analytical results.

PACS numbers: 83.10.Pp,47.15.G-,47.55.Kf,47.10.-g

I. INTRODUCTION

The angular motion of a neutrally buoyant spheroid in a simple shear has recently been studied extensively and in detail at moderately large shear Reynolds numbers, by numerical stability analysis and by computer simulations using the lattice-Boltzmann method[1–6]. The results show that particle and fluid inertia give rise to intricate angular dynamics. At moderate and large Reynolds numbers a large number of bifurcations distinguish many different periodic orbits and fixed points.

At zero shear Reynolds number particle and fluid inertia are negligible, and the angular dynamics is determined by an infinite set of marginally stable periodic orbits, the so-called Jeffery orbits[7].

The effect of weak fluid and particle inertia on the angular motion of a neutrally buoyant spheroid in a simple shear was analysed recently[8–12]. In Refs. 8–11 an approximate angular equation of motion was derived for arbitrary aspect ratios of the spheroidal particle, and valid to linear order in the shear Reynolds number. Linear stability analysis of the Jeffery orbits subject to infinitesimal inertial perturbations allowed to determine the linear stability of the log-rolling orbit (where the particle symmetry axis is aligned with vorticity), and of tumbling in the flow-shear plane: log rolling was found to be unstable for prolate spheroids and stable for oblate spheroids, in agreement with the results obtained by Subramanian and Koch [12] in the slender-body limit. Refs. 8–11 predicted that tumbling in shear plane is stable for prolate spheroids. For oblate spheroids tumbling was found to be stable for very flat disks, otherwise unstable. An earlier attempt to compute the stability of log rolling of nearly spherical particles yields results that are at variance with the results stated above[13]. This fact and further literature is discussed by Einarsson *et al.* [9].

In the present paper we analyse the stability of the log-rolling orbit numerically at finite but small shear Reynolds numbers by discretising the coupled particle-flow problem directly. We find good agreement with the analytical results of Refs. 9–11 in the limit where the shear Reynolds number tends to zero, and when the system size tends to infinity. The numerical method allows to determine corrections to the analytical results, and to compute the effect of confinement.

To numerically determine the stability of the tumbling orbit we use lattice-Boltzmann simulations and find the bifurcations of the tumbling orbit at small shear Reynolds numbers. At the smallest Re_a attained ($\mathrm{Re}_a = 1$) the bifurcation occurs at a critical aspect ratio of $\lambda_\mathrm{c} \approx 0.1275$ in the finite system, in qualitative agreement with the analytical results obtained for an unbounded system. In order to obtain quantitative agreement lattice-Boltzmann simulations at smaller shear Reynolds numbers and in larger systems are required.

We briefly comment on the wider context of this paper. Recently there has been a surge of interest in describing the tumbling of small non-spherical particles in turbulent[14–20] and complex flows[21–23] using Jeffery's equation. Studies of the dynamics of larger non-spherical particles in turbulence[14,19,24] take into account particle inertia but neglect fluid inertia because it is difficult to solve the coupled particle-flow problem. For heavy particles this may be a good approximation, but the results summarised in this paper (and the results of Refs. 3,5,6,9–12) show that this is approximation is likely to fail for neutrally buoyant and nearly neutrally buoyant particles.

The remainder of this paper is organised as follows. Section II describes the coupled particle-flow problem that is the subject of this paper. In Section III we summarise the analytical results of Refs. 9–11 and find the bifurcations of the angular equation of motion obtained in these references. Our numerical results are described in Section IV, and compared to the analytical results. Section V contains our conclusions.

II. FORMULATION OF THE PROBLEM

The problem has the following dimensionless parameters. The shape of the spheroid is determined by the shape factor Λ defined as $\Lambda = (\lambda^2-1)/(\lambda^2+1)$ where λ is aspect ratio of spheroid, $\lambda = a/b$ for prolate spheroids, a is the major semi-axis length of the particle, and b is the minor semi-axis length. For oblate spheroids the aspect ratio is defined as $\lambda = b/a$. The effect of fluid inertia is measured by the shear Reynolds number $\mathrm{Re}_a = a^2 s/\nu$ where ν is the kinematic viscosity of the fluid and s is the shear rate. Particle inertia is measured by the Stokes number, $\mathrm{St} = (\rho_\mathrm{p}/\rho_\mathrm{f})\mathrm{Re}_a$ where ρ_p and ρ_f are particle and fluid mass densities. The numerical computations described in this paper are performed in a finite system of linear size L, and $\kappa = 2a/L$ is a dimensionless measure of the system size, $2a$ is the length of the major axis of the particle.

We use dimensionless variables to formulate the problem[9–11]. The length scale is taken to be the major semi-axis length a of the spheroid. The velocity scale is as, the pressure scale is μs, and force and torque scales are $\mu s a^2$ and $\mu s a^3$ respectively, μ is the dynamic viscosity of the fluid. In dimensionless variables the angular equations of motion read

$$\dot{\boldsymbol{n}} = \boldsymbol{\omega} \wedge \boldsymbol{n}\,, \quad \mathrm{St}\,\dot{\boldsymbol{L}} = \mathrm{St}\,(\mathbb{I}\dot{\boldsymbol{\omega}} + \dot{\mathbb{I}}\boldsymbol{\omega}) = \boldsymbol{T}\,. \tag{1}$$

Here $\boldsymbol{n}$ is the unit vector along the particle symmetry axis, dots denote time derivatives, $\mathbb{I} = A^I(\mathbb{1} - \mathbb{P}_\perp) + B^I\mathbb{P}_\perp$ is the particle-inertia matrix, $\mathbb{P}_\perp$ is a projector onto the plane perpendicular to $\boldsymbol{n}$ with elements $P_{ij} = \delta_{ij} - n_i n_j$, and A^I and B^I are moments of inertia along and orthogonal to $\boldsymbol{n}$. The particle angular velocity is $\boldsymbol{\omega}$, and $\boldsymbol{T}$ is the hydrodynamic torque:

$$\boldsymbol{T} = \int_{\mathscr{S}} \boldsymbol{r} \wedge \boldsymbol{\sigma}\mathrm{d}\boldsymbol{s}\,. \tag{2}$$

The integral is over the particle surface $\mathscr{S}$, and $\boldsymbol{\sigma}$ is the stress tensor with elements $\sigma_{ij} = -p\delta_{ij} + 2S_{ij}$ where p is pressure, and S_{ij} are the elements of the strain-rate matrix $\mathbb{S}$, the

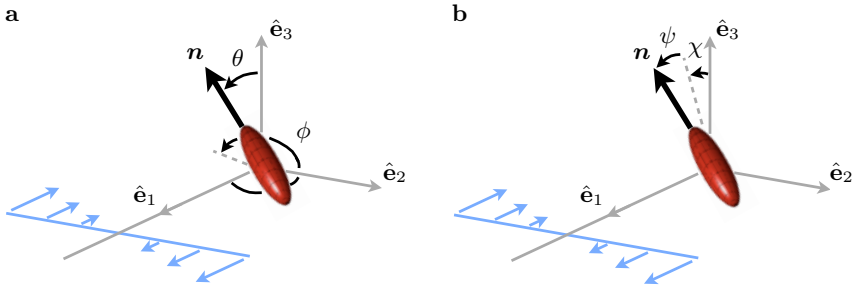

FIG. 1. Schematic illustration of spheroid in a simple shear in a coordinate system that translates with centre of mass of the particle. Vorticity points along the negative $\hat{\mathbf{e}}_3$-axis, and $\hat{\mathbf{e}}_1$ is the flow direction. The flow-shear plane is spanned by $\hat{\mathbf{e}}_1$ and $\hat{\mathbf{e}}_2$. We use two different coordinate systems to express the orientation of the unit vector $\boldsymbol{n}$ aligned with the symmetry axis of the particle. **a** Spherical coordinate system used for analysing linear stability of tumbling in the shear plane, θ is the polar angle from the vorticity axis, and ϕ is the azimuthal angle in the flow-shear plane. **b** Spherical coordinate system used for analysing linear stability of log rolling, $\boldsymbol{n} = [0, 0, 1]$ corresponds to $\chi = \psi = 0$.

symmetric part of the matrix $\mathbb{A}$ of fluid-velocity gradients with elements $A_{ij} = \partial_j u_i$ (u_i are the components of the fluid velocity $\boldsymbol{u}$). The anti-symmetric part of $\mathbb{A}$ is denoted by $\mathbb{O}$ with elements O_{ij}. To determine the torque it is necessary to solve the Navier-Stokes equations for the incompressible fluid:

$$\mathrm{Re}_a\big(\partial_t \boldsymbol{u} + (\boldsymbol{u}\cdot\boldsymbol{\nabla})\boldsymbol{u}\big) = -\boldsymbol{\nabla} p + \Delta\boldsymbol{u}\,, \quad \nabla\cdot\boldsymbol{u} = 0\,. \tag{3}$$

For a neutrally buoyant particle $\mathrm{Re}_a = \mathrm{St}$.

It is assumed that the slip velocity vanishes on the particle surface $\mathscr{S}$, $\boldsymbol{u} = \boldsymbol{\omega}\wedge\boldsymbol{r}$ when $\boldsymbol{r}\in\mathscr{S}$, where $\boldsymbol{r}$ denotes the position vector. The perturbation calculations Refs. 9–11 apply to a simple shear in an unbounded system, and it is assumed that the fluid velocity far from the particle is unaffected by its presence: $\boldsymbol{u}=\boldsymbol{u}^\infty$ as $|\boldsymbol{r}|\to\infty$. Here $\boldsymbol{u}^\infty$ denotes the velocity field of the simple shear $\boldsymbol{u}^\infty = \mathbb{A}^\infty\boldsymbol{r}$ with $A^\infty_{ij} = \delta_{i1}\delta_{j2}$ (see Fig. 1 for an illustration of the geometry). The symmetric and antisymmetric parts of $\mathbb{A}^\infty$ are denoted by $\mathbb{S}^\infty$ and $\mathbb{O}^\infty$, respectively.

The numerical computations described in this paper pertain to a finite system, a cube of linear size L. In the shear direction $\boldsymbol{u} = \pm\kappa^{-1}$ at $r_2 = \pm\kappa^{-1}$. Tomas: please check. In the flow and vorticity directions periodic boundary conditions with spatial period L are used. Tomas: briefly mention wall boundary conditions. Say: no significant difference.

The coupled non-linear particle-flow problem is determined by Eqs. (1) to (3) and the boundary conditions stated above. In the creeping-flow limit the dynamics of $\boldsymbol{n}$ was found by Jeffery [7]. In this limit there are infinitely many degenerate periodic orbits, the so-called Jeffery orbits. Which particular periodic orbit the vector $\boldsymbol{n}$ follows is determined by the initial orientation. But inertial effects change the stability of the Jeffery orbits, as discussed in the two following Sections.

III. THEORY AT SMALL Re_a.

In Refs. 9–11 an approximate angular equation of motion was derived, valid to linear order in $\mathrm{Re}_a = \mathrm{St}$:

$$\begin{aligned}\dot{\boldsymbol{n}} = {}& \mathbb{O}^\infty\boldsymbol{n} + \Lambda[\mathbb{S}^\infty\boldsymbol{n} - (\boldsymbol{n}\cdot\mathbb{S}^\infty\boldsymbol{n})\boldsymbol{n}] + \beta_1(\boldsymbol{n}\cdot\mathbb{S}^\infty\boldsymbol{n})\mathbb{P}_\perp\mathbb{S}^\infty\boldsymbol{n} \\ & + \beta_2(\boldsymbol{n}\cdot\mathbb{S}^\infty\boldsymbol{n})\mathbb{O}^\infty\boldsymbol{n} + \beta_3\,\mathbb{P}_\perp\mathbb{O}^\infty\mathbb{S}^\infty\boldsymbol{n} + \beta_4\,\mathbb{P}_\perp\mathbb{S}^\infty\mathbb{S}^\infty\boldsymbol{n}\,.\end{aligned} \tag{4}$$

The first two terms on the r.h.s. of this equation are Jeffery's result for a neutrally buoyant spheroid in the creeping-flow limit. The remaining terms are corrections due to particle and fluid inertia. The four coefficients β_α (for $\alpha = 1,\ldots,4$) are linear in Re_a and St but

TABLE I. Asymptotic behaviour of the functions $b_\alpha(\lambda) = \beta_\alpha/\mathrm{Re}_a$ where β_α are the coefficients in Eq. (4) for $\mathrm{St} = \mathrm{Re}_a$. The asymptotes are found by expanding the solutions from Refs. 9,10.

	prolate $\lambda \to \infty$	oblate $\lambda \to 0$
b_1	$\frac{7}{15(2\log\lambda-3+\log 4)} + \frac{-197\log 2\lambda+92\log\lambda\log 4\lambda+106+92(\log 2)^2}{15\lambda^2(2\log\lambda-3+\log 4)^2}$	$\frac{11}{30}+\big(\frac{176}{45\pi}-\frac{7\pi}{20}\big)\lambda+\big(-\frac{7}{3}+\frac{3968}{135\pi^2}-\frac{21\pi^2}{80}\big)\lambda^2$
b_2	$\frac{1}{5(2\log\lambda-3+\log 4)} + \frac{(\log\lambda-1+\log 2)(8\log 2\lambda-7)}{5\lambda^2(2\log\lambda-3+\log 4)^2}$	$\frac{1}{10}+\big(\frac{8}{15\pi}-\frac{\pi}{20}\big)\lambda+\big(-\frac{1}{5}+\frac{128}{45\pi^2}-\frac{3\pi^2}{80}\big)\lambda^2$
b_3	$-\frac{4}{5\lambda^2}$	$-\frac{1}{5}+\frac{9\pi^2-64}{60\pi}\lambda+\big(\frac{3}{5}-\frac{256}{45\pi^2}+\frac{9\pi^2}{80}\big)\lambda^2$
b_4	$\frac{4}{15\lambda^2}$	$-\frac{1}{3}+\big(\frac{\pi}{20}-\frac{64}{45\pi}\big)\lambda+\big(\frac{5}{3}-\frac{1024}{135\pi^2}+\frac{3\pi^2}{80}\big)\lambda^2$

non-linear functions of the particle aspect ratio λ: $\beta_\alpha = b_\alpha^{(\mathrm{Re}_a)}(\lambda)\mathrm{Re}_a + b_\alpha^{(\mathrm{St})}(\lambda)\mathrm{St}$. These functions were computed by Einarsson *et al.*[9,10] for general values of λ, and in Ref. 11 in the nearly-spherical limit. Eq. (4) determines the effect of small inertial perturbations on the Jeffery orbits. It turns out that log-rolling ($\boldsymbol{n}$ aligned with the vorticity axis) and tumbling in the flow-shear plane survive small inertial perturbations. In the following two Sections we discuss the linear stabilities of these two orbits, for $\mathrm{St} = \mathrm{Re}_a$. We write $\beta_\alpha = \mathrm{Re}_a\, b_\alpha(\lambda)$. Table I gives the asymptotes of these functions for large and small values of the aspect ratio λ. The asymptotes are obtained by expanding the results derived in Ref. 10.

A. Linear stability analysis of log rolling

To analyse the stability of the log-rolling orbit we use the coordinate system shown in Fig. 1**b**. The angles χ and ψ are defined so that

$$n_1 = \sin\psi\,, \quad n_2 = \cos\psi\sin\chi\,, \quad n_3 = \cos\psi\cos\chi\,. \tag{5}$$

In these coordinates the equation of motion (4) takes the form:

$$\begin{aligned}\dot\psi &= \frac{1}{8}\big[4(\Lambda\cos 2\psi+1)\sec\psi\sin\chi \\ &\quad + \big(4\beta_1\cos 2\psi\sin^2\chi + (-2\beta_2-\beta_3+\beta_4)\cos 2\chi + 2\beta_2+3\beta_3+\beta_4\big)\sin\psi\big]\cos\psi\,, \qquad (6a)\\ \dot\chi &= \frac{1}{8}\big[2(\Lambda-1)\tan\psi + \big((\beta_2-\beta_1)\cos 2\psi+\beta_1-\beta_2-\beta_3+\beta_4\big)\sin\chi\big]\cos\chi\,. \qquad (6b)\end{aligned}$$

Log rolling along the vorticity direction $\boldsymbol{n} = [0,0,1]$ corresponds to $\chi = \psi = 0$, and this is a fixed point of Eq. (6) since $\dot\psi = \dot\chi = 0$ in this direction. The stability of this fixed point is determined by the eigenvalues of the linearisation of Eq. (6) around this fixed point. To linear order in Re_a the eigenvalues take the form

$$\gamma_{\mathrm{LR}}^{\pm} = \frac{\beta_4}{4} \pm \frac{\mathrm{i}}{2}\sqrt{1-\Lambda^2} + o(\mathrm{Re}_a)\,. \tag{7}$$

We see that the fixed point is a spiral, and that its stability is determined by β_4. This coefficient is positive for prolate spheroids (unstable log rolling) and negative for oblate spheroids (stable log rolling). The real part of Eq. (7) is linear in Re_a, its form was derived in Refs. 9,10, see for example Fig. 3**a** in Ref. 9. The imaginary part corresponds to Jeffery's frequency[7]. It has no linear-Re_a correction.

B. Tumbling in the shear plane

To analyse tumbling in the shear plane we use the coordinates employed in Refs. 9–11 (illustrated in Fig. 1**a**):

$$n_1 = \sin\theta\cos\phi\,, \quad n_2 = \sin\theta\sin\phi\,, \quad n_3 = \cos\theta\,. \tag{8}$$

In these coordinates the equation of motion (4) takes the form

$$\dot\phi = \frac{1}{2}\left(\Lambda\cos 2\phi - 1\right) + \frac{1}{8}\beta_1\sin^2\theta\sin 4\phi - \frac{1}{4}\sin 2\phi\left(\beta_2\sin^2\theta + \beta_3\right)\,, \tag{9a}$$

$$\dot\theta = \Lambda\sin\theta\cos\theta\sin\phi\cos\phi + \frac{1}{4}\sin\theta\cos\theta\left(\beta_1\sin^2\theta\sin^2 2\phi + \beta_3\cos 2\phi + \beta_4\right)\,. \tag{9b}$$

This is Eq. (42) in Ref. 9. Eq. (9b) shows that $\dot\theta = 0$ at $\theta = \pi/2$, in the flow-shear plane. The equation of motion for ϕ in this plane is

$$\dot\phi = \frac{1}{2}\left(\Lambda\cos 2\phi - 1\right) + \frac{1}{8}\beta_1\sin 4\phi - \frac{1}{4}(\beta_2+\beta_3)\sin 2\phi\,. \tag{10}$$

For sufficiently small values of Re_a there is a periodic tumbling orbit in the shear plane because $\dot\phi < 0$. Its linear stability exponent γ_T at infinitesimal shear Reynolds numbers was calculated in Refs. 9,10. It was found that tumbling in the shear plane is stable for prolate particles in this limit, and unstable for not too thin oblate particles. For very thin platelets tumbling was found to be stable.

As Re_a increases we see that $\dot\phi \geq 0$ in Eq. (9) for some value(s) of ϕ. This implies the existence of fixed points in the flow-shear plane. This happens in Eq. (9) for any aspect ratio. Jonas, Bernhard: comment on that Eq. (9) must fail at larger Re_a. Therefore look only at limits where the bifurcation occurs at small Re_a. Can't be sure at which Re_a Eq. (9) fails to faithfully represent the actual dynamics but this is the best we can do. The bifurcation occurs at small Re_a only for thin rods and plates.

Consider first rods. Rods of infinite aspect ratio align with the flow direction, particles with finite aspect ratio tumble at infinitesimal Re_a. At finite values of Re_a a bifurcation may cause a rod with finite aspect ratio to align. To find this bifurcation point we expand $\dot\phi$ to second order in $1/\lambda$ (Table I) and to second order in ϕ. A double root of the resulting quadratic equation for ϕ determines the bifurcation point:

$$\mathrm{Re}_a^{(\mathrm{c1})} \sim \frac{15}{\lambda}\big(-3 + \log 4 + 2\log\lambda\big) \quad \text{as } \lambda\to\infty\,. \tag{11}$$

This result for $\mathrm{Re}_a^{(\mathrm{c1})}$ is consistent with Eq. (3.31) in Ref. 12 (up to a factor of 8π). Subramanian and Koch [12] derived their result using the slender-body approximation. Note that the qualitative features of the dynamics in the vicinity of $\mathrm{Re}_a^{(\mathrm{c1})}$ are consistent with Eq. (12) in Ref. 25 (see also Zettner and Yoda [26]). As $\varepsilon \equiv \mathrm{Re}_a - \mathrm{Re}_a^{(\mathrm{c1})}$ tends to zero from below the period of the tumbling orbit tends to infinity as $(-\varepsilon)^{-1/2}$. Above the transition there are two fixed points, one unstable and one stable. It follows that the particle aligns at the angle

$$\phi_0 = \frac{1}{\lambda} + \frac{\sqrt{\varepsilon}}{15}\frac{\sqrt{30}}{\sqrt{\lambda(-3+\log 4+2\log\lambda)}} + \ldots \quad \text{as } \lambda\to\infty, \tag{12}$$

for small values of ε. Up to a factor of 8π this is consistent with Eqs. (3.30) and (3.31) in Ref. 12.

Now we turn to thin disks. The symmetry vector of an infinitely thin disk aligns with the shear direction, $\dot\phi = 0$ for $\phi = \pi/2$ when $\lambda = 0$. For non-zero values of λ the vector $\boldsymbol{n}$ tumbles in the flow-shear plane in the limit of $\mathrm{Re}_a \to 0$. At finite (but small) values of Re_a a bifurcation may cause the disk to align. To find this bifurcation point we expand $\dot\phi$ to

second order in λ (Table I) and to second order in $\delta\phi = \phi - \pi/2$. As above a double root of the resulting quadratic equation for $\delta\phi$ determines the critical shear Reynolds number:

$$\mathrm{Re}_a^{(\mathrm{c}2)} \sim 15\lambda \quad \text{as } \lambda \to 0\,. \tag{13}$$

For $\mathrm{Re}_a > \mathrm{Re}_a^{(\mathrm{c}2)}$ the symmetry vector $\boldsymbol{n}$ of the disk aligns in the flow-shear plane at the angle

$$\phi_0 = \frac{\pi}{2} + \lambda + \frac{\sqrt{\epsilon}}{15}\sqrt{30\lambda} \quad \text{as } \lambda \to 0. \tag{14}$$

In deriving this expression only the lowest orders in λ and ϵ were kept.

For larger values of λ there is a critical λ_c where the tumbling orbit changes stability. At infinitesimal shear Reynolds numbers the linear stability exponent of the tumbling orbit is of the form $\gamma_\mathrm{T} = h_1(\lambda)\mathrm{Re}_a + o(\mathrm{Re}_a)$. The function h_1 is derived from the solutions obtained in Refs. 9,10. We do not write it down because the expression is lengthy. At infinitesimal Re_a the bifurcation point is determined by $h_1(\lambda_\mathrm{c}) = 0$. Einarsson *et al.*[9,10] found

$$\lambda_\mathrm{c} \approx 0.137\,. \tag{15}$$

The bifurcation lines in the λ-Re_a-plane given by Eqs. (11), (13), and (15) are shown in Fig. 4. This figure also contains the results of our direct numerical simulations (DNS) which we discuss next.

IV. NUMERICAL COMPUTATIONS

We performed different types of DNS of Eqs. (1) to (3) in a finite domain with velocity boundary conditions in the shear direction, periodic boundary conditions in the other directions, and no-slip boundary conditions on the particle surface. We directly computed the linear stability of the log-rolling orbit using version 4.4 of the commercial software package Comsol Multiphysics$^{\mathrm{TM}}$. As explained below this method could not be used to numerically determine the linear stability of tumbling in the shear plane. Therefore we used lattice-Boltzmann simulations of the particle dynamics to determine the bifurcations of this orbit. To check the accuracy of the lattice-Boltzmann simualtions we also performed steady-state DNS using version 9.06 of the commercial software package STAR-CCM+$^{\mathrm{TM}}$.

A. Direct numerical stability analysis of log rolling at finite values of Re_a

The eigenvalue solver in version 4.4 of the commercial finite-element software package Comsol Multiphysics$^{\mathrm{TM}}$,[27] makes it possible to analyse the stability of the log-rolling orbit as described in this Section. The symmetries of the problem ensure that log rolling exists not only at infinitesimal but also at finite shear Reynolds numbers (Jonas: please say this more precisely).

A common way of simulating the dynamics of a solid particle in a fluid is to employ a fixed Eulerian grid for the fluid and an immersed Lagrangian grid for the particle. In order to accurately resolve the boundary layer around the particle at finite values of Re_a the fluid grid must be refined close to the particle surface. This can be very time consuming and may require re-meshing as the particle rotates. This explains why the log-rolling orbit is much simpler to analyse than other orbits: log rolling is a fixed point of the dynamics of the vector $\boldsymbol{n}$ aligned with the symmetry axis of the particle. To determine the linear stability of this fixed point it is sufficient to account for small deviations of $\boldsymbol{n}$ from the fixed point, and for the fact that the particle spins around its symmetry axis.

The analysis proceeds in two steps. The first step is to find the steady-state solution of Eqs. (1) to (3) for a given value of Re_a, keeping $\boldsymbol{n}$ fixed in the log-rolling direction, $\boldsymbol{n} = [0, 0, 1]$. This determines the angular velocity $\boldsymbol{\omega}$ at which the particle spins around its

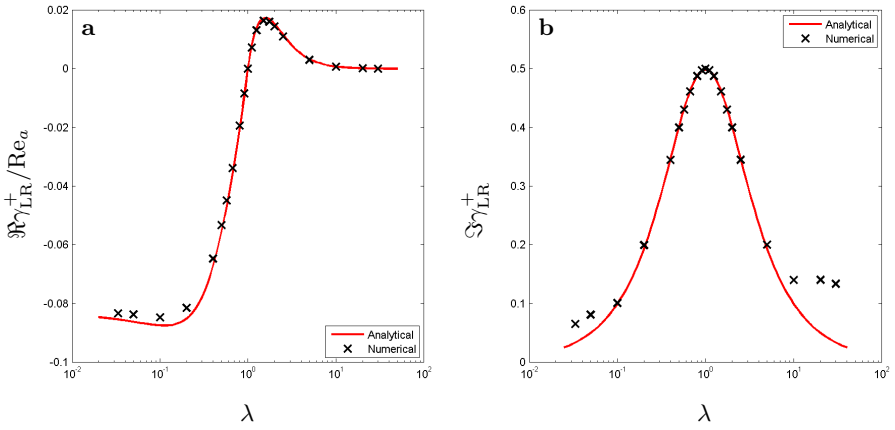

FIG. 2. **a** Comparison between the analytical result (7) for $\Re\gamma^+_{\rm LR}$ (solid red line) and numerical results (black crosses) from direct numerical stability analysis (Section IV A). Parameters: ${\rm Re}_a = 2.5\cdot10^{-4}$ and $\kappa = 0.025$. **b** Same comparison for the imaginary part $\Im\gamma^+_{\rm LR}$.

symmetry axis. The second step is to allow for infinitesimal deviations of $\boldsymbol{n}$ and $\boldsymbol{\omega}$ from this steady state. We use a so-called 'arbitrary Lagrangian-Eulerian method'[27] for grid refinement close to the particle surface, linearise the resulting dynamics, and determine the eigenvalues of the linearised problem using the eigenvalue solver in Comsol, which is based on ARPACK FORTRAN routines for large eigenvalue problems[27,28]. In our case the linearisation is a sparse (Tomas please check, is it sparse?) matrix of linear dimension 10^5. Correct? The eigenvalue solver provides N eigenvalues $\gamma_1,\ldots,\gamma_N$ closest to the origin in the complex plane, ordered by ascending real parts, $\Re\gamma_1 > \ldots > \Re\gamma_N$.

When the shear Reynolds number is small we usually find that N–2 eigenvalues $\gamma_3,\ldots,\gamma_N$ are real (within numerical accuracy) with negative real parts. These are fluid modes that decay rapidly as the steady state is approached. In addition there is one leading pair of complex conjugate eigenvalues $\gamma_{1,2}$ with largest real part. This complex pair corresponds to the linear stability exponent $\gamma^\pm_{\rm LR}$ of the log-rolling orbit. It can have positive or negative real part, and the imaginary part determines the angular velocity of the particle. We must choose N large enough to ensure that this pair is among the N eigenvalues the solver finds. In most cases we found $N = 200$ to be sufficient. At larger values of ${\rm Re}_a$ it may happen that fluid modes have real parts that are larger than that of $\gamma^\pm_{\rm LR}$, yet they are still real (within numerical accuracy). When this happens we verify that the complex pair describes the stability of the orientational dynamics of the particle by numerically integrating the dynamics near the steady state.

In this way we determined $\gamma^\pm_{\rm LR}$ as a function of the particle aspect ratio λ for different degrees κ of confinement, and for different values of ${\rm Re}_a$. Fig. 2 shows real and imaginary parts of $\gamma^\pm_{\rm LR}$ as functions of the aspect ratio of the particle, for a small shear Reynolds number in a large system (${\rm Re}_a = 2.5\cdot10^{-4}$ and $\kappa = 0.025$). Fig. 2**a** compares the numerical results for the real part of $\gamma_{\rm LR}$ with the theory, Eq. (7). We observe excellent agreement. This lends support to the analytical results of Refs. 9–12, and also to the numerical linear stability analysis. Fig. 2**b** compares numerical results for the imaginary part $\Im\gamma^+_{\rm LR}$ with Eq. (7). Also here good agreement is observed, at least for moderate aspect ratios $\lambda \in [10^{-1}, 10]$. For more extreme aspect ratios it is likely that the grid is not fine enough to resolve the high curvature along the particle rim.

Fig. 3**a** shows finite-${\rm Re}_a$ corrections to $\Re\gamma^+_{\rm LR}$ for $\lambda = 2$ and for the smallest value of κ at which we could reliably compute, $\kappa = 0.025$. Also shown is a fit to

$$\Re\gamma_{\rm LR} = a_1(\lambda,\kappa)\,{\rm Re}_a + a_2(\lambda,\kappa)\,{\rm Re}_a^{3/2}\,. \tag{16}$$

The values obtained for the coefficients a_1 and a_2 are listed in Table II, together with

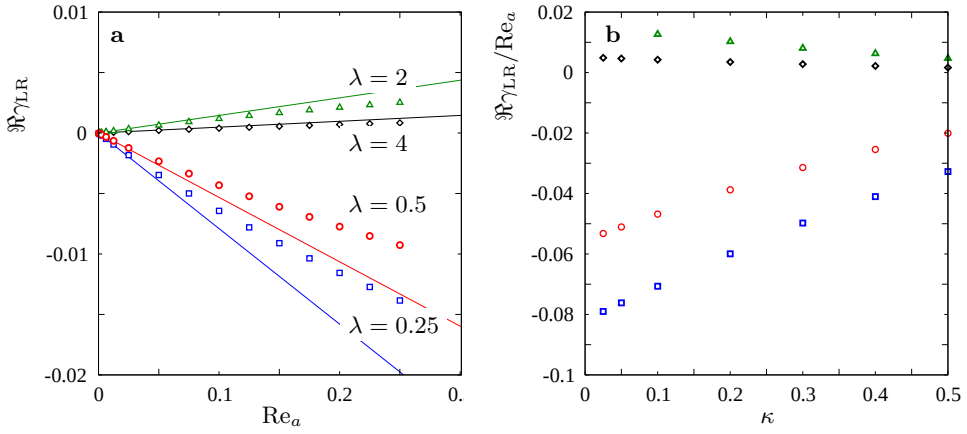

FIG. 3. **a** Shows $\Re\gamma^+_{\rm LR}$ as a function of Re_a for $\kappa = 0.025$ and four different values of λ. The thin solid lines show the limiting behaviour as $\mathrm{Re}_a \to 0$. Bernhard: The thick solid lines show fits to Eq. (16). The coefficients are given in Table II. **b** Finite-size corrections to $\Re\gamma^+_{\rm LR}/\mathrm{Re}_a$ for $\mathrm{Re}_a = 0.25 \cdot 10^{-4}$ and the same values of λ as in panel **a**.

TABLE II. Shows the coefficients a_1 and a_2 from the fit (16) to the data shown in Fig. 3 for $\lambda = 2$ and $\kappa = 0.025$, as well as the coefficients obtained from fits to numerical data for other values of λ (not shown in Fig. 3). Also given are the numerical values for $b_4(\lambda)/4$ (Ref. 9) to which the coefficients a should converge as $\kappa \to 0$.

λ	a_1	$b_4(\lambda)/4$	a_2
1/4			
1/2			
2	0.0149	0.0153	0.0089
4			

the corresponding values for other aspect ratios. We expect a $\mathrm{Re}_a^{3/2}$-correction to Eq. (7): in deriving Eq. (7) using the reciprocal theorem the integrand in one of the terms (that has Re_a as a multiplicative factor) was approximated by the Stokes solution corresponding to our problem. But there are corrections to the Stokes solution far away from particle. Further than Ekman length $2a/\mathrm{Re}_a^{1/2}$ the actual solution decays more rapidly than the Stokes solution[29,30]. We expect that this results in a $\mathrm{Re}_a^{3/2}$-correction to $\gamma_{\rm LR}$ provided that the system is large enough, $\kappa \ll \mathrm{Re}_a^{1/2}$.

Tomas: one paragraph on 'mode chaos' that results when Re_a too large. At which Re_a does this occur for $\lambda = 2$ and $\kappa = 0.025$?

Fig. 3**b** shows finite-size corrections to $\Re\gamma^+_{\rm LR}$ for $\mathrm{Re}_a = 2.5 \cdot 10^{-4}$ and $\lambda = 2$. Also shown is a linear fit. It does not describe the κ-dependence very well, but we could not obtain data for small enough κ to check whether the finite-size corrections are linear in κ as $\kappa \to 0$.

B. Time-resolved lattice-Boltzmann simulations

To analyse the bifurcations of the tumbling in the shear plane we use the lattice Boltzmann method with external boundary force[31]. In this method a Lagrangian grid for the particle is immersed in an Eulerian fluid grid. It turns out that the grid resolutions of the Lagrangian and Eulerian grids should be chosen to be approximately the same to obtain most accurate results In its present form the algorithm employs an Eulerian fluid grid with uniform resolution, the same close to the particle and far from it. This prevents us from resolving the fluid close to the particle very well while at the same time keeping the system size κ^{-1} large. We have thus simulated only moderate system sizes, $\kappa^{-1} = 5$. This allows us to resolve the particle with at least six fluid grid-nodes along its smallest dimension. To restrict the computational time, the domain size is set to a maximum of $L = 240$ lattice units. These choices limit the range of aspect ratios that can be simulated to $\lambda \in [1/8, 8]$.

Note also that the lattice-Boltzmann model is based upon kinetic theory. It describes an incompressible fluid provided that the Knudsen number $\mathrm{Kn} = \nu/(ac_{\mathrm{LB}})$ and the Mach number $\mathrm{Ma} = as/c_{\mathrm{LB}}$ are small enough, $c_{\mathrm{LB}} = \sqrt{1/3}$ lattice units per time step is the sound speed of the model. In our simulations we require that $\mathrm{Ma} < 0.035$ and $\mathrm{Kn} < 0.014$. To increase the shear Reynolds number above $\mathrm{Re}_a = \mathrm{Ma}/\mathrm{Kn} = 2.5$ we decrease the Knudsen number, to decrease the Reynolds number below 2.5 we decrease the Mach number. Since a and c_{LB} are kept constant the shear rate s is decreased to reach small Re_a. But since the shear rate is proportional to the discrete time step size, it becomes computationally very expensive to reach small values of Re_a. With these considerations in mind (also discussed by Rosén *et al.*[5,6]) we decided to take $\mathrm{Re}_a \geq 0.5$ in our simulations. To estimate the critical aspect ratio λ_{c} where tumbling changes stability for oblate particles we proceeded as follows. We initialized the particle at rest, close to the tumbling orbit at $\phi = \pi/2$ and $\theta = \pi/2 - \delta\theta$ with $\delta\theta = 0.017$. We integrated the dynamics for aspect ratios $\lambda = 1/8, 1/7, 1/6, 1/5, 1/4$, and for Re_a between 1 and 10 with unit increments. We determined whether the tracjetory tended to tumbling in the shear plane or to the log-rolling orbit, and determined the location of the bifurcation by interpolation. At $\mathrm{Re}_a = 1$ we ran simulations for λ ranging between 0.125 and 0.160 with increments of 0.05 and determined the bifucation point by linear interpolation. The results are illustrated in Fig. 4. We see that the results agree fairly well with Eq. (15). At the smallest value of Re_a simulated, the transition occurs at $\lambda_c \approx 0.0125$, not too far from the analytical result (15) at infinitesimal Re_a.

We also used lattice-Boltzmann simulations to obtain estimates for $\mathrm{Re}_a^{(\mathrm{c1})}$ and $\mathrm{Re}_a^{(\mathrm{c2})}$ (Section III). This was done by initialising the particle at rest at $\phi = \pi/4$ and $\theta = \pi/2$ for $\lambda > 1$ and at $\phi = 3\pi/4$ and $\theta = \pi/2$ for $\lambda < 1$. We then determined whether the particle tended to a steady state or continued to tumble, and determined the critical Reynolds number by linear interpolation. The results of these simulations are also shown in Fig 4, and are compared with the analytical results for thin disks and rods given by Eqs. (11) and (13). We find that the agreement is only qualitative, but note that the lattice-Boltzmann simulations were performed for a rather small system, while the analytical results pertain to an unbounded system. To check the accuracy of the lattice-Boltzmann simulations we determined the critical Reynolds numbers $\mathrm{Re}_a^{(\mathrm{c1})}$ and $\mathrm{Re}_a^{(\mathrm{c2})}$ using an alternative approach, described in the next Section.

C. Steady-state simulations using STAR-CCM+™

The critical Reynolds numbers $\mathrm{Re}_a^{(\mathrm{c1})}$ and $\mathrm{Re}_a^{(\mathrm{c2})}$ can be determined from steady-state numerical simulations using version 9.06 of the commercial finite-volume software package STAR-CCM+™[32]. We used this package to determine the steady-state torque that the fluid exerts on the particle and located where in the λ-Re_a plane this torque vanishes, given that the particle symmetry vector lies in the flow-shear plane. We proceeded as follows. We chose the same system size as in the lattice-Boltzmann simulations, $\kappa^{-1} = 5$. The particle orientation was fixed at $\theta = \pi/2$, $\phi \in [0, \pi/2]$ for prolate particles, and $\phi \in [\pi/2, \pi]$ for

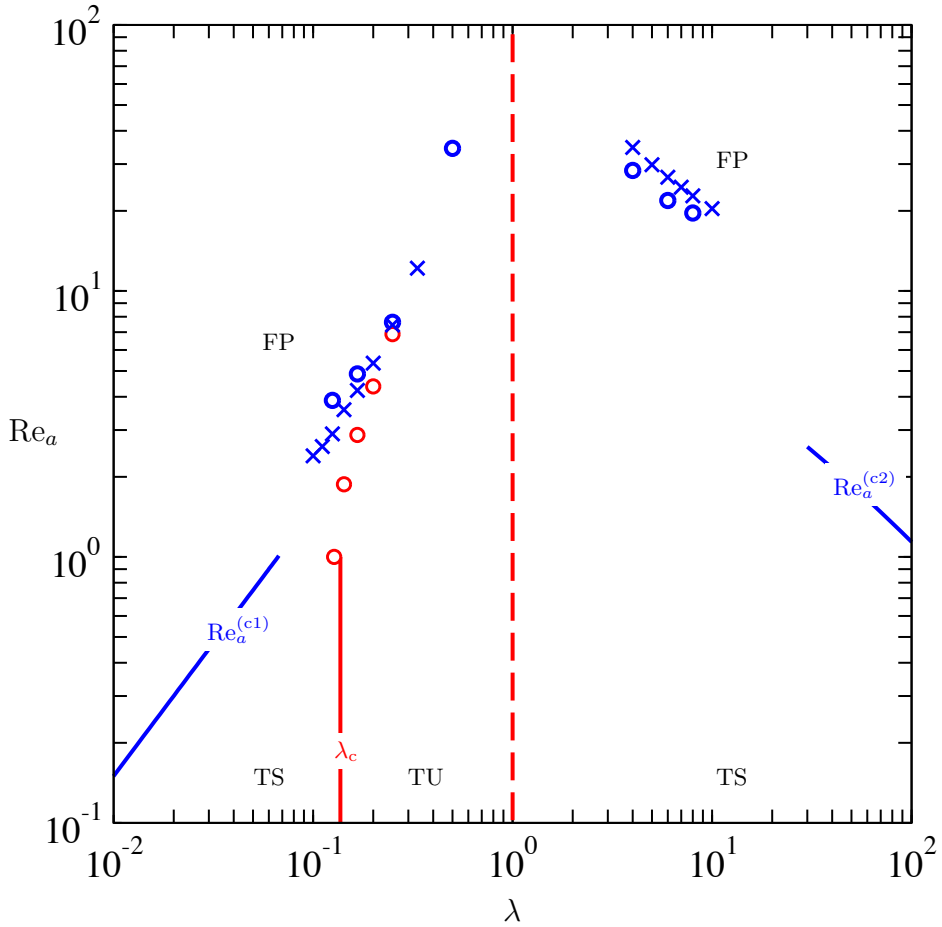

FIG. 4. Bifurcation diagram of the tumbling orbit in the λ-Re_a-plane. Bifurcation lines derived in Section III – Eqs. (11), (13), and (15) – are shown as solid lines. The label TS indicates that tumbling is stable, TU that it is unstable, and FP that the tumbling orbit has bifurcated to a fixed point corresponding to a fixed orientation in the flow-shear plane. The dashed line denotes the symmetry line at λ where the tumbling orbit changes stability. The numerical results at $\kappa^{-1} = 5$ are shown as symbols: ($\circ$) denote results from the time-resolved lattice-Boltzmann simulations in described in Section IV B, ($\times$) represent results from the steady-state simulations described in Section IV C. The bifurcations where tumbling in the shear plane changes stability are shown in red, the bifurcations where stable tumbling in the shear plane changes to a stable fixed point are shown in blue. Tomas please check: caption for blue crosses and blue circles correct? Doesn't appear to be consistent.

oblate particles. A fixed particle orientation allowed to use a very fine local grid around the particle. For different choices of ϕ we found critical Reynolds numbers where the steady-state torque vanishes. The minimum of this critical Reynolds as a function of ϕ gives $\mathrm{Re}_a^{(c1)}$ or $\mathrm{Re}_a^{(c2)}$, for oblate and prolate particles respectively. The corresponding results for $\mathrm{Re}_a^{(c1)}$ and $\mathrm{Re}_a^{(c2)}$ are also shown in Fig. 4. We conclude that the lattice-Boltzmann simulations slightly under-predict the critical value $\mathrm{Re}_a^{(c1)}$, while they slightly over-predict $\mathrm{Re}_a^{(c2)}$. Not consistent with caption of Fig. 4.

V. CONCLUSIONS

Using numerical linear stability analysis we computed the stability of the log-rolling orbit of a neutrally buoyant spheroid in a simple shear at small Re_a. For infinitesimally small

Re_a this problem was recently solved for arbitrary aspect ratios using perturbation theory in the shear Reynolds number. The fact that both calculations agree in the limits $\mathrm{Re}_a \to 0$ and $\kappa \to 0$ (unbounded system) lends support to the analytical calculations[9–12], but also to the numerical linear stability analysis described in the present article. In the limit of large system size ($\kappa \to 0$) we found that corrections to the analytical result for the exponent $\Re\gamma^+_{\mathrm{LR}}$ are of order $\mathrm{Re}_a^{3/2}$. We also investigated finite-size corrections to $\Re\gamma^+_{\mathrm{LR}}$ at small Re_a, and found that they are substantial. It would be of interest to calculate both finite-Re_a and finite-size corrections to $\Re\gamma^+_{\mathrm{LR}}$ by extending the method used in Refs. 9–12.

We did not investigate the stability of the tumbling orbit with numerical linear stability analysis because the required re-meshing is computationally very expensive. Instead we studied the stability of tumbling in the shear plane using lattice-Boltzmann simulations. Following the bifurcation line between stable/unstable tumbling for thin oblate spheroids (solid red line in Fig. 4) down to as small values of Re_a as we can reliably achieve and find that the transition occurs at $\lambda_{\mathrm{c}} \approx 0.125$ at $\mathrm{Re}_a = 0.875$, in fair agreement with the theoretical prediction 0.137.

Finally we determined under which circumstances tumbling in the flow-shear plane bifurcates to a fixed point, using lattice-Boltzmann simulations, and also by numerically computing steady-state torques using STAR-CCM+$^{\mathrm{TM}}$. The two numerical procedures give results that are in fairly good agreement with each other, yet the agreement with the analytical results (11) and (13) is only qualitative. This could be due to the fact that the numerical simulations were performed for a rather small system, while the analytical calculations are for an unbounded shear. But it must also be borne in mind that Eqs. (11) and (13) were obtained by bifurcation analysis of an approximate equation: Eq. (4) is valid to linear order in Re_a only.

Detailed analysis of the lattice-Boltzmann dynamics near the bifurcation at $\mathrm{Re}_a^{(\mathrm{c1})}$ reveals the phase-space topology near the bifurcation at moderate Reynolds numbers ($\mathrm{Re}_a^{(\mathrm{c1})} \approx 7.8$ at $\lambda = 1/4$), see Fig. 3(d),(e) in Ref. 6. For $\lambda = 1/4$ a second bifurcation occurs at $\mathrm{Re}_a \approx 5$ where the log-rolling orbit changes from stable spiral to stable node. Eq. (4) also exhibits this bifurcation. But since Eq. (4) is valid to linear order in Re_a the bifurcation can only be analysed in the limit $\lambda \to 0$. In this limit we find that the two bifurcations occur in reverse order: the tumbling→fixed point bifurcation occurs before the spiral→node bifurcation as the shear Reynolds number is increased. Inspection shows that the phase-space topology is slightly different too. Describe difference in bifurcation of unstable limit cycle at $\mathrm{Re}_a^{(\mathrm{c1})}$ at $\lambda = 1/4$ (Rosén *et al.*[6]) and in the limit $\lambda \to 0$. One sentence. There are several possible explanations for these subtle differences. They could be due to higher-order Re_a-corrections to Eq. (4) such as the $\mathrm{Re}_a^{3/2}$-corrections alluded to above. It cannot be excluded that finite-size corrections play a role.

In summary we can conclude that the results of our numerical computations agree well with the theoretical predictions at infinitesimal Reynolds numbers: we find excellent agreement for the stability exponent of the log-rolling orbit, and the bifurcation of the tumbling orbit for thin oblate particles occurs in both theory and simulations, at similar values of λ_{c}. But there are a number of subtle differences between theory and simulations at larger Reynolds numbers. It is unlikely that the lattice-Boltzmann simulations can be reliably performed at much smaller shear Reynolds numbers than we have managed to do. Therefore it would be of great interest to extend the analytical calculations to include $\mathrm{Re}_a^{3/2}$-corrections and to account for finite-size effects.

ACKNOWLEDGMENTS

JE and BM acknowledge support by Vetenskapsrådet and by the grant 'Bottlenecks for particle growth in turbulent aerosols' from the Knut and Alice Wallenberg Foundation, Dnr. KAW 2014.0048. We might add some other acknowledgements here.

[1]D. Qi and L. Luo, "Rotational and orientational behaviour of three-dimensional spheroidal particles in Couette flows," J. Fluid Mech. **477**, 201 (2003).
[2]H. Huang, X. Yang, M. Krafczyk, and X.-Y. Lu, "Rotation of spheroidal particles in Couette flows," J. Fluid Mech. **692**, 369–394 (2012).
[3]T. Rosén, F. Lundell, and C. K. Aidun, "Effect of fluid inertia on the dynamics and scaling of neutrally buoyant particles in shear flow," J. Fluid Mech. **738**, 563–590 (2014).
[4]W. Mao and W. Alexeev, "Motion of spheroid particles in shear flow with inertia," J. Fluid Mech. **749**, 145 (2014).
[5]T. Rosén, M. Do-Quang, C. Aidun, and F. Lundell, "The dynamical states of a prolate spheroidal particle suspended in shear flow as a consequence of particle and fluid inertia," J. Fluid Mech. **771**, 115–158 (2015).
[6]T. Rosén, M. Do-Quang, C. Aidun, and F. Lundell, "Effect of fluid and particle inertia on the rotation of an oblate spheroidal particle suspended in linear shear flow," Phys. Rev. E (2015).
[7]G. B. Jeffery, "The motion of ellipsoidal particles immersed in a viscous fluid," Proceedings of the Royal Society of London. Series A **102**, 161–179 (1922).
[8]J. Einarsson, J. R. Angilella, and B. Mehlig, "Orientational dynamics of weakly inertial axisymmetric particles in steady viscous flows," Physica D: Nonlinear Phenomena **278–279**, 79–85 (2014).
[9]J. Einarsson, F. Candelier, F. Lundell, J. Angilella, and B. Mehlig, "Rotation of a spheroid in a simple shear at small Reynolds number," Phys. Fluids **27**, 063301 (2015).
[10]J. Einarsson, F. Candelier, F. Lundell, J. Angilella, and B. Mehlig, "Effect of weak fluid inertia upon Jeffery orbits," Phys. Rev. E **91**, 041002(R) (2015).
[11]F. Candelier, J. Einarsson, F. Lundell, B. Mehlig, and J. Angilella, "The role of inertia for the rotation of a nearly spherical particle in a general linear flow," Phys. Rev. E **91**, 053023 (2015).
[12]G. Subramanian and D. L. Koch, "Inertial effects on fibre motion in simple shear flow," Journal of Fluid Mechanics **535**, 383–414 (2005).
[13]P. G. Saffman, "On the motion of small spheroidal particles in a viscous liquid," J. Fluid Mech. **1**, 540 (1956).
[14]C. Marchioli, M. Fantoni, and A. Soldati, "Orientation, distribution, and deposition of elongated, inertial fibers in turbulent channel flow," Phys. Fluids **22**, 033301 (2010).
[15]S. Parsa, E. Calzavarini, F. Toschi, and G. A. Voth, "Rotation rate of rods in turbulent fluid flow," Phys. Rev. Lett. **109**, 134501 (2012).
[16]A. Pumir and M. Wilkinson, "Orientation statistics of small particles in turbulence," NJP **13**, 093030 (2011).
[17]R. Ni, N. T. Ouelette, and G. A. Voth, "Alignment of vorticity and rods with Lagrangian fluid stretching in turbulence," J. Fluid Mech. **743**, R3 (2014).
[18]L. Chevillard and C. Meneveau, "Orientation dynamics of small, triaxial-ellipsoidal particles in isotropic turbulence," J. Fluid Mech. **737**, 571 (2013).
[19]N. R. Challabotla, L. Zhao, and H. Andersson, "Orientation and rotation of inertial disk particles in wall turbulence," J. Fluid Mech. **766**, R2 (2015).
[20]M. Byron, J. Einarsson, K. Gustavsson, G. Voth, B. Mehlig, and E. Variano, "Shape-dependence of particle rotation in isotropic turbulence," Phys. Fluids (2015).
[21]M. Wilkinson, V. Bezuglyy, and B. Mehlig, "Fingerprints of random flows," Phys. Fluids **21**, 043304 (2009).
[22]V. Bezuglyy, B. Mehlig, and M. Wilkinson, "Poincaré indices of rheoscopic visualisations," Europhys. Lett. **89**, 34003 (2010).
[23]M. Wilkinson, V. Bezuglyy, and B. Mehlig, "Emergent order in rheoscopic swirls," J. Fluid Mech. **667**, 158 (2011).
[24]K. Gustavsson, J. Einarsson, and B. Mehlig, "Tumbling of small axisymmetric particles in random and turbulent flows," Phys. Rev. Lett. **112**, 014501 (2014).
[25]E.-J. Ding and C. K. Aidun, "The dynamics and scaling law for particles suspended in shear flow with inertia," J. Fluid Mech. **423**, 317 (2000).
[26]C. M. Zettner and M. Yoda, "Moderate-aspect-ratio elliptical cylinders in simple shear with inertia," J. Fluid Mech. **442**, 241 (2001).
[27]*Comsol Multiphysics^{TM} Reference Manual, version 4.4* (www.comsol.com, 2013).
[28]*http://www.caam.rice.edu/software/ARPACK/*.
[29]P. Lovalenti and J. Brady, "The force on a bubble, drop or particle in arbitrary time-dependent motion at small Reynolds number." Phys. Fluids **5**, 2104–2116 (1993).
[30]F. Candelier, J.-R. Angilella, and M. Souhar, "On the effect of inertia and history forces on the slow motion of a spherical solid or gaseous inclusion in a solid-body rotation flow," J. Fluid Mech. **545**, 113–139 (2013).
[31]J. Wu and C. K. Aidun, "Simulating 3d deformable particle suspensions using lattice Boltzmann method with discrete external boundary force," Int. J. Numer. Meth. Fl. **62**, 765 (2010).
[32]*STAR-CCM+*.